A Novel Reference Signal Based on the OCDM Scheme for a PLC Channel Measurement Methodology

Ian do A. Pimenta, Lucas Giroto de Oliveira, Mateus de L. Filomento, Thomas Zwick, Moisés V. Ribeiro, and Ândrei Camponogara

***Abstract*— This paper presents an orthogonal chirp-division multiplexing (OCDM)-based reference signal intended for implementation in a power line communication (PLC) channel measurement methodology, paired with the Schmidl & Cox symbol block synchronization scheme. The performance of this proposal is assessed through numerical comparisons with a discrete multitone (DMT) modulation-based reference signal, focusing on synchronization point estimation and peak-to-average power ratio (PAPR). The obtained results indicate that while the OCDM-based reference signal parallels the DMT-based one in terms of synchronization point estimation, it also offers the advantage of a reduced PAPR.**

***Keywords*— Measurement methodology, orthogonal chirp-division multiplexing, power line communication, sounding, synchronization.**

I. Introduction

Power line communication (PLC) systems present a compelling solution as they eliminate the need for expensive infrastructure deployment and inherently provide capillarity [1]. However, since electric power systems were not originally intended for communication, information-carrying signals may experience significant degradation. This may manifest as exponential attenuation increases with frequency and distance, multipath effects due to impedance mismatching, and high-power impulsive noise resulting from dynamic loads. Consequently, estimating channel frequency responses (CFRs) in PLC systems is a complex task because of the necessity to account for the degradation in the transmitted signals [2].

In [2], a PLC channel measurement methodology utilizing a sounding approach was proposed, with the reference signal used for channel estimation composed of successive discrete multitone (DMT) symbols. Subsequently, [3] adapted this methodology, employing the synchronization scheme suggested by Schmidl Cox [4], which exhibits greater robustness than the scheme discussed in [2]. It's important to note that both [2], [3] employed the DMT scheme, potentially resulting in a transmission signal with high peak-to-average power ratio (PAPR), which could undermine the measurement methodology's effectiveness. One alternative is the orthogonal chirp-division multiplexing (OCDM) scheme, which has been demonstrated as a viable and robust alternative to the established orthogonal frequency-division multiplexing (OFDM) and DMT schemes [5], [6]. In this context, Filomeno *et. al* [7] proposed a unique OCDM pilot symbol intended to work with the synchronization scheme of Schmidl Cox. However, introducing the OCDM symbol block alone does not suffice for creating a reference signal for the channel measurement methodology, as it still necessitates two uncorrelated symbol blocks [2].

To address the aforementioned problems, this paper proposes an OCDM-based reference signal, compatible with the PLC channel measurement methodology delineated in [2], [3]. The proposed reference signal consists of the OCDM pilot symbol introduced in [7], supplemented by a modified OCDM pilot symbol. Finally, to evaluate the performance of the proposed reference signal in terms of symbol synchronization and PAPR, numerical results are presented, offering a comparison with the reference signal described in [3].

The rest of the paper is organized as follows. Section II details the PLC channel measurement methodology. Section III introduces the DMT-based reference signal. Section IV presents the proposed OCDM-based reference signal. Section V discusses the numerical results. Finally, Section VI provides some concluding remarks.

II. Measurement Methodology

The PLC channel measurement methodology encompasses several stages that facilitate the estimation of PLC channels via the sounding procedure. As shown in Fig. 1, a reference signal is created at the transmitter and injected into the electric power grid via a capacitive coupling circuit. This signal is then subjected to waveform distortion as a result of its propagation through the electric power grid and is further corrupted by the presence of high-power additive noise. The receiver subsequently captures the resultant signal through another coupling circuit connected to the electric power grid.

Ian do A. Pimenta and Ândrei Camponogara are with the Department of Electrical Engineering, Federal University of Paraná, Curitiba, PR, Brazil (e-mails:iamaralpimenta@gmail.com, andrei.camponogara@ufpr.br).

Lucas Giroto de Oliveira and Thomas Zwick are with the Institute of Radio Frequency Engineering and Electronics, Karlsruhe Institute of Technology, Karlsruhe, Germany (e-mail: {lucas.oliveira, thomas.zwick}@kit.edu).

Mateus de L. Filomeno and Moisés V. Ribeiro are with the Department of Electrical Engineering, Federal University of Juiz de Fora, Juiz de Fora, MG, Brazil (e-mails: {mateus.lima, mribeiro}@engenharia.ufjf.br).

This research was supported in part by Coordenação de Aperfeiçoamento de Pessoal de Nível Superior (CAPES) under Grant 001, Conselho Nacional de Desenvolvimento Científico e Tecnológico (CNPq) under grants 404068/2020-0 and 314741/2020-8, Fundação de Amparo à Pesquisa do Estado de Minas Gerais (FAPEMIG) under grants APQ-03609-17, TEC-PPM 00787-18, and APQ-04623-22, and Instituto Nacional de Energia Elétrica (INERGE).

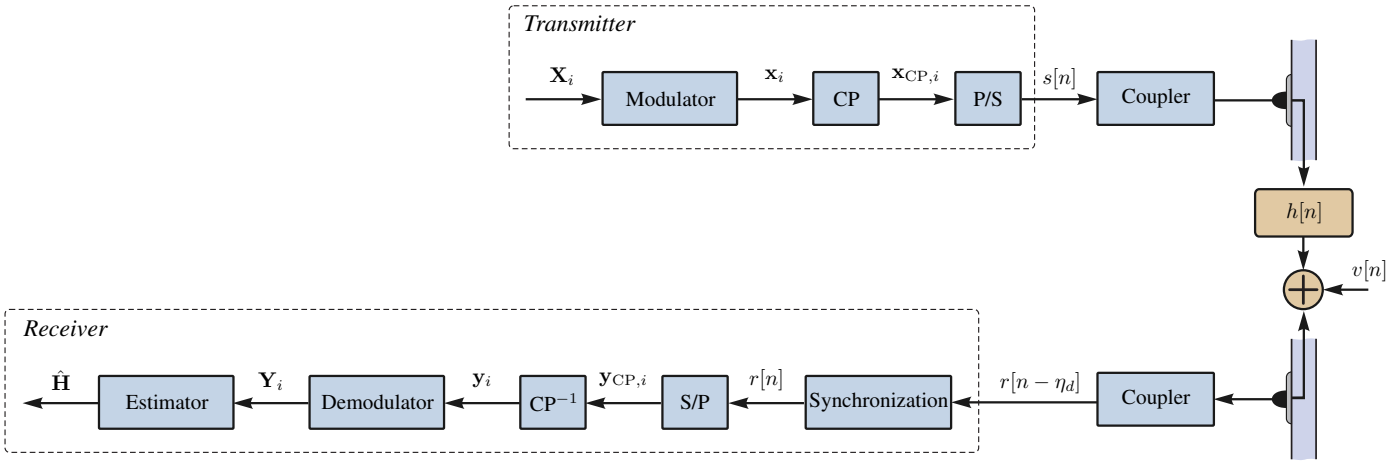

Fig. 1. Block diagram illustrating a simplified representation of the PLC channel measurement methodology in the discrete-time domain.

Following the synchronization process, and given that the receiver is familiar with the reference signal, the received signal can be demodulated, allowing for the estimation of the PLC channel.

In the PLC channel measurement methodology, synchronization comprises two critical steps: symbol block synchronization and sampling frequency estimation and correction. This paper focuses solely on symbol block synchronization, thus assuming perfect sampling frequency estimation and correction. The objective of the symbol block synchronization scheme is to precisely estimate the reference signal's initial point at the receiver to prevent intersymbol interference (ISI) and facilitate effective PLC channel estimation. Consistent with [3], we employ the Schmidl & Cox synchronization scheme [4], which requires each symbol block of the reference signal to have identical halves in the time domain. However, the presence of additive noise, inherent in data communication media, may compromise the performance of the symbol block synchronization. To mitigate this, successive estimates for the reference signal's initial point can be computed and averaged. This requires the generation of two uncorrelated symbol blocks, forming the transmission frame $\mathbf{s}_f = [\mathbf{x}_{\mathrm{CP},1}^T\, \mathbf{x}_{\mathrm{CP},2}^T]^T$, where $(\cdot)^T$ is the transpose operator and $\mathbf{x}_{\mathrm{CP},1}, \mathbf{x}_{\mathrm{CP},2} \in \mathbb{R}^{(N+L_{\mathrm{CP}})\times 1}$ represents uncorrelated symbol blocks, each with an appended cyclic prefix (CP). Consequently, the reference signal in the discrete-time domain can be represented as

$$s[n] = \sum_{i=-\infty}^{\infty} \sum_{j=0}^{2(N+L_{\mathrm{CP}})-1} s_{f,j}\delta[n-j-i2(N+L_{\mathrm{CP}})], \quad (1)$$

in which $\delta[n]$ is the Kronecker delta and $s_{f,j}$ is the j^{th} element of the vector $\mathbf{s}_f$.

The received signal in the discrete-time domain can be expressed as

$$r[n-\eta_d] = \sum_{m=-\infty}^{\infty} s[m]h[n-\eta_d-m] + v[n], \quad (2)$$

in which $\{h[n]\}_{n=0}^{L_h-1}$ is the PLC channel impulse response (CIR) with length L_h, $\{v[n]\}$ represents the additive noise, and η_d is a random variable representing the time delay between the received signal and the local temporal reference at the receiver. Moreover, PLC channel estimates are assumed to be obtained within the coherence time. In other words, $\{h[n]\}_{n=0}^{L_h-1}$ is considered as the impulse response of a linear and time-invariant system.

Now, one intends to estimate the initial reference point $\hat{n}$ (or synchronization point) to remove η_d from $\{r[n-\eta_d]\}$. Notice that a good synchronization point estimate is the one that is located within the so-called ISI-free region, which spans in the interval $[L_h, L_{\mathrm{CP}}]$. By using the Schmidl & Cox synchronization scheme, two L-length correlation windows separated by L samples slide over the sequence $\{r[n]\}$ and provide the necessary information to calculate the so-called normalized correlation function, which is given by [4]

$$M[n] = \frac{\left|\sum_{l=0}^{L-1}(r[n+l]r[n+l+L])\right|^2}{\left(\sum_{l=0}^{L-1}|r[n+l+L]|^2\right)^2}. \quad (3)$$

As illustrated in Fig. 2, the normalized correlation function periodically takes the shape of a plateau in the ISI-free region. The period of $\{M[n]\}$ is L and the synchronization point estimation $\hat{n}_m$ associated with the m^{th} period of $\{M[n]\}$ can be obtained by finding the midpoint in the existing plateau in the m^{th} period of $\{M[n]\}$. To mitigate the additive noise effect, the estimation of the synchronization point is calculated by averaging the midpoints of the K consecutive plateaus, i.e.,

$$\hat{n} = \frac{1}{K}\sum_{m=0}^{K-1}\hat{n}_m - m(N+L_{\mathrm{CP}}). \quad (4)$$

Lastly, details about the estimation process and the reference signal based on DMT- and OCDM are provided in Sections III and IV, respectively.

III. DMT-Based Reference Signal

This section details the DMT-based reference signal addressed in [3]. As discussed in Section II, this reference signal uses two uncorrelated DMT symbol blocks with two equal halves each to allow the use of the Schmidl & Cox

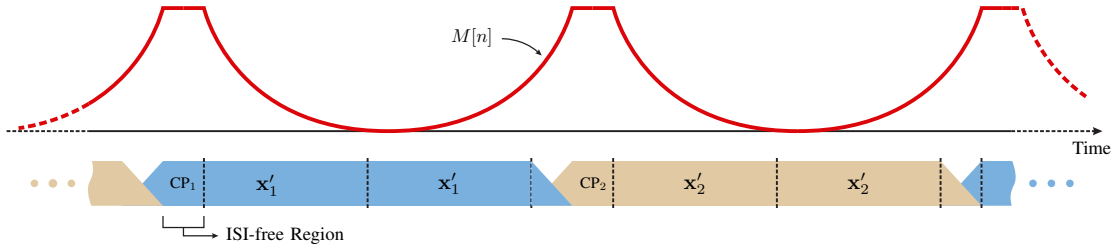

Fig. 2. An example of a normalized correlation function curve $\{M[n]\}$ obtained from a DMT-based signal reference.

synchronization scheme. To generate the reference signal based on the DMT scheme, first, symbols from an M-ary constellation are allocated at the even positions of the vector $\mathbf{X}_i \in \mathbb{C}^{N/2\times 1}$ whereas the odd positions are made null, i.e., $\mathbf{X}_i = [X_i[0]\ 0\ X_i[2]\ \cdots\ X_i[N/2-2]\ 0]^T$. Then $\mathbf{X}_i$ is mapped according to the Hermitian symmetric rule addressed in [8], which yields $\mathbf{X}_{\mathrm{MP},i} \in \mathbb{C}^{N\times 1}$. After applying the normalized version of the inverse discrete Fourier transform (IDFT), one has $\mathbf{x}_i = \mathbf{F}^\dagger \mathbf{X}_{\mathrm{MP},i}$ with $\mathbf{F} = \mathbf{W}/\sqrt{N}$ being the N-size normalized discrete Fourier transform (DFT) matrix and $(\cdot)^\dagger$ denoting the Hermitian operator. Note that due to the null odd elements of $\mathbf{X}_i$, $\mathbf{x}_i$ has two equal halves, i.e., $\mathbf{x}_i = [\mathbf{x}_i'^T\ \mathbf{x}_i'^T]^T$ with $\mathbf{x}_i' \in \mathbb{R}^{N/2\times 1}$, which is demanded by the Schmidl & Cox synchronization scheme. Next, an L_{CP}-length CP is prepended to the symbol block, and the result is the vector $\mathbf{x}_{\mathrm{CP},i} = [x_i'[N/2-L_{\mathrm{CP}}]\ x_i'[N/2-L_{\mathrm{CP}}+1]\ \cdots\ x_i'[N/2-1]\ x_i'[0]\ x_i'[1]\ \cdots\ x_i'[N/2-1]]^T$. Two distinct symbols are equally generated to form $\mathbf{s}_f = [\mathbf{x}_{\mathrm{CP},1}^T\ \mathbf{x}_{\mathrm{CP},2}^T]^T$.

After a succeeded synchronization process, the CP is removed, and then the normalized DFT is applied to each symbol block. Consequently, the vector representation of the received signal in the frequency domain is given by

$$\mathbf{Y}_i = \mathbf{\Lambda}_{\mathbf{X}_{\mathrm{MP},i}}\mathbf{H} + \mathbf{V}_i, \tag{5}$$

where $\mathbf{\Lambda}_{\mathbf{X}_{\mathrm{MP},i}} = \mathrm{diag}\{X_{\mathrm{MP},i}[0],\ X_{\mathrm{MP},i}[1],\ \cdots,\ X_{\mathrm{MP},i}[N-1]\}$ is the diagonal matrix of $\mathbf{X}_{\mathrm{MP},i}$, $\mathbf{H} \in \mathbb{C}^{N\times 1}$ is the vector representation of the PLC CFR, and $\mathbf{V}_i \in \mathbb{C}^{N\times 1}$ is the vector representation of the additive noise in the frequency domain. For channel estimation, it is assumed that the symbol block $\mathbf{X}_{\mathrm{MP},i}$ is known at the receiver. Thus, the $\mathbf{H}$ estimate can be obtained from the received signal $\mathbf{Y}_i$. Mathematically, the CFR estimate can be expressed as

$$\begin{aligned}\hat{\mathbf{H}} &= \mathbf{\Lambda}^{-1}_{\mathbf{X}_{\mathrm{MP},i}}\mathbf{\Lambda}_{\mathbf{X}_{\mathrm{MP},i}}\mathbf{H} + \mathbf{\Lambda}^{-1}_{\mathbf{X}_{\mathrm{MP},i}}\mathbf{V}_i \\ &= \mathbf{H} + \mathbf{\Lambda}^{-1}_{\mathbf{X}_{\mathrm{MP},i}}\mathbf{V}_i.\end{aligned} \tag{6}$$

Then the vector representation of a PLC CIR estimate is given by

$$\hat{\mathbf{h}} = \mathbf{W}^\dagger \hat{\mathbf{H}}, \tag{7}$$

with $\hat{\mathbf{h}} \in \mathbb{R}^{N\times 1}$.

IV. The Proposed OCDM-Based Reference Signal

This section introduces an OCDM-based reference signal, which is based on the OCDM pilot symbol block addressed in [7]. In this sense, let $\dot{\mathbf{x}}_i \in \mathbb{R}^{N\times 1}$ represents the discrete-Fresnel symbol block. Then $\mathbf{x}_i = \mathbf{\Phi}\dot{\mathbf{x}}_i$ is the version $\dot{\mathbf{x}}_i$ in the discrete-time domain, where $\mathbf{\Phi} = \mathbf{F}^\dagger\mathbf{\Gamma}\mathbf{F}$ is the discrete Fresnel transform (DFnT) matrix and $\mathbf{\Gamma} = \mathrm{diag}\{\Gamma[0],\ \Gamma[1],\ \cdots,\ \Gamma[N-1]\}$ is the diagonal matrix of the eigenvalues of $\mathbf{\Phi}$. Assuming that N is even, for a baseband transmission, the k^{th} element of $\mathbf{\Gamma}$ can be expressed as [6]

$$\Gamma[k] = \begin{cases} e^{-(j2\pi/N)k^2}, & \text{for } k < N/2 \\ e^{(j2\pi/N)k^2}, & \text{for } k \geq N/2. \end{cases} \tag{8}$$

To generate the reference signal based on the OCDM scheme, the authors propose two pilot symbol blocks in the discrete-Fresnel domain, $\dot{\mathbf{x}}_1$ and $\dot{\mathbf{x}}_2$. According to [7], these symbol blocks must have two equal halves in the discrete-Fresnel domain so that they also have two equal halves in the discrete-time domain, enabling the Schmidl & Cox symbol synchronization scheme. Following [7], the authors suggest the k^{th} element/subchirp of the first OCDM symbol block $\dot{\mathbf{x}}_1 \in \mathbb{R}^{N\times 1}$ to be designed as

$$\dot{x}_{1,k} = \delta[k] + \delta\left[k - \frac{N}{2}\right] \tag{9}$$

with $k = 0,\ 1,\ \cdots,\ N-1$.

The second symbol block $\dot{\mathbf{x}}_2 \in \mathbb{R}^{N\times 1}$, on the other hand, must be designed to be decorrelated from $\dot{\mathbf{x}}_1$. Therefore, the authors propose the k^{th} element/subchirp of the second symbol block $\dot{\mathbf{x}}_1 \in \mathbb{C}^{N\times 1}$ to be given by using frequency shift precoding (FPS) [9]

$$\dot{x}_{2,k} = \dot{x}_{1,k}e^{\frac{j2\pi k}{N}} \tag{10}$$

with $k = 0,\ 1,\ \cdots,\ N-1$. Note that similar to the discrete-time domain, the multiplication of a sequence in the discrete-Fresnel domain by the sequence $\{e^{\frac{j2\pi k}{N}}\}$ results in one sample shift in the frequency domain. Consequently, after applying the DFnT matrix in both symbol blocks, the respective symbol blocks can be obtained in the discrete-time domain as

$$\mathbf{x}_1 = [\mathbf{x}_1'^T\ \mathbf{x}_1'^T]^T \quad \text{and} \quad \mathbf{x}_2 = [\mathbf{x}_2'^T\ \mathbf{x}_2'^T]^T,$$

where $\mathbf{x}_1', \mathbf{x}_2' \in \mathbb{R}^{N/2\times 1}$. After prepending a CP to each symbol block, the reference signal is formed by concatenating the two symbol blocks, with the transmission frame being given by

$$\mathbf{s}_f = [\mathbf{x}_{\mathrm{CP},1}^T\ \mathbf{x}_{\mathrm{CP},2}^T]^T. \tag{11}$$

At the receiver, after synchronization, the CP is removed and then the DFnT is applied to each symbol block. Due to the convolution preservation property of the DFnT [5], the vector representation of the received signal in the discrete-Fresnel domain can be expressed as

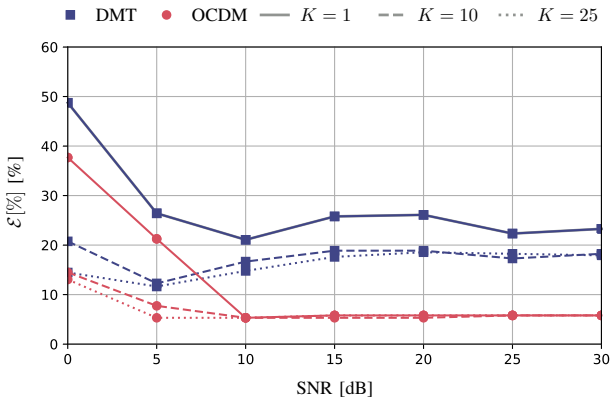

Fig. 3. Mean estimation error in percentage, $\mathcal{E}[\%]$, as a function of the SNR of the synchronization point estimates for both DMT- and OCDM-based reference signals.

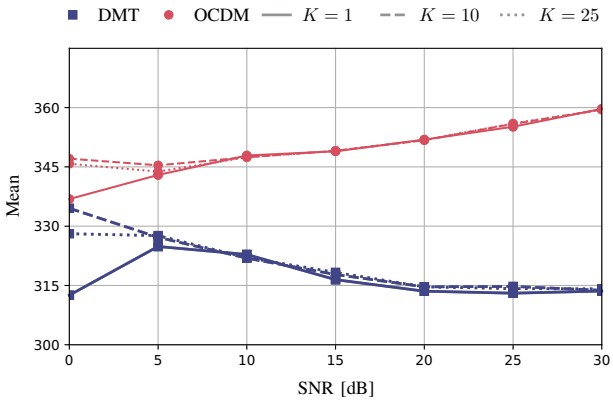

Fig. 4. Mean value of the synchronization point estimates as a function of the SNR for DMT- and OCDM-based reference signals.

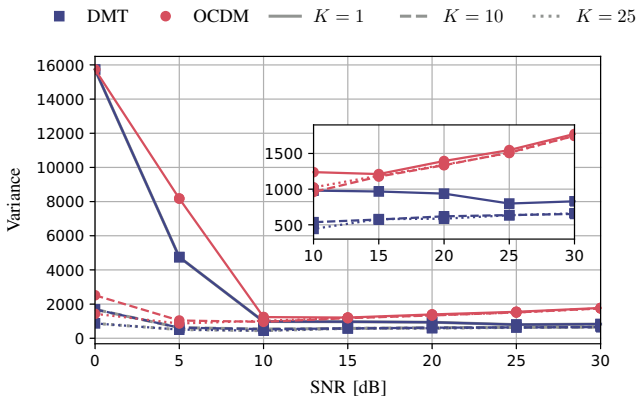

Fig. 5. Variance of the synchronization point estimates as a function of the SNR for both DMT- and OCDM-based reference signals.

$$\begin{aligned}\mathbf{Y}_i &= \mathbf{h}_{\text{c}}\dot{\mathbf{x}}_i + \dot{\mathbf{v}}_i \\ &= \tilde{\mathbf{Y}}_i + \dot{\mathbf{v}}_i,\end{aligned} \tag{12}$$

in which $\mathbf{h}_{\text{c}} \in \mathbb{R}^{N\times N}$ stands for the circulant matrix for the vector $\mathbf{h}$, i.e., the PLC CIR, and $\dot{\mathbf{v}}_i \in \mathbb{C}^{N\times 1}$ represents the additive noise in the discrete-Fresnel domain. As long as $L_h \leq N/2$, it holds that $\tilde{\mathbf{Y}}_i = [\mathbf{h}^T\ \mathbf{0}_{N/2-L_h}\ \mathbf{h}^T\ \mathbf{0}_{N/2-L_h}]^T$ for $\dot{\mathbf{x}}_i = \dot{\mathbf{x}}_1$, where $\mathbf{0}_a$ denotes a row vector of a zeros. Therefore, a PLC CIR estimate can be obtained by averaging the two halves of $\mathbf{Y}_i$. If $\dot{\mathbf{x}}_i = \dot{\mathbf{x}}_2$, then a simple phase multiplication by $e^{-\frac{j2\pi k}{N}}$ can be applied to similarly acquire a PLC CIR estimate.

V. Numerical Results

This section evaluates the performance of the proposed OCDM-based reference signal and a comparison with the DMT-based one in [3]. To generate the numerical results, a data set of 343 PLC channel estimates obtained in the measurement campaign reported in [10] was considered. The reference signals based on the DMT and OCDM schemes are generated considering $N = 4096$ and $L_{\text{CP}} = 512$ according to [2], [3]. Also, binary-phase shift keying (BPSK) symbols are taken into account to generate the two DMT symbol blocks.

Moreover, the performance is evaluated in terms of the mean estimation error in percentage, mean, and variance of the synchronization point estimates considering $K \in \{1, 10, 25\}$ symbol blocks. Note that the mean estimation error in percentage is calculated by

$$\mathcal{E}[\%] = \frac{100}{I}\sum_{i=0}^{I-1}\epsilon_i, \tag{13}$$

in which

$$\epsilon_i = \begin{cases} 0, & L_h \leq \hat{n} \leq L_{\text{CP}} \\ 1, & \text{otherwise,} \end{cases} \tag{14}$$

and I is the number of channels for which the estimates $\hat{n}$ are calculated.

Fig. 3 depicts $\mathcal{E}[\%]$ as a function of the SNR for $K \in \{1, 10, 25\}$, considering the DMT- and OCDM-based reference signals. For $K = 1$ and low SNR values, a relatively high mean error for both reference signals are observed. As the SNR and the number of symbol blocks (estimates) increase, an expected reduction of $\mathcal{E}[\%]$ can be noticed, and it can also be seen that $\mathcal{E}[\%]$ for each reference signal follows the same trend up to SNR $=$ 30 dB. Lastly, Fig. 3 evidences that for SNRs higher than 10 dB, the OCDM scheme provides the lowest $\mathcal{E}[\%]$ values regardless of the number of estimates.

Figs. 4 and 5 show respectively the mean and variance values of $\hat{n}$ as a function of the SNR for the DMT- and OCDM-based reference signals. The plot of the mean value in Figs. 4 shows that $\hat{n}$ does not change significantly for the DMT- and OCDM-based reference signals as the SNR increases; however, mean values for both reference signals remain within the ISI-free plateau, regardless of the SNR or K values. The analysis of the plots in Fig. 5 reveals that for SNR $\in [0, 5]$ dB and $K = 1$, the variance of $\hat{n}$ is high, almost $16,000$. Whereas, for the same SNR values, but considering $K > 1$, the variances of $\hat{n}$ are lower than $2,500$. As the SNR increases, the difference between the variances for different values of K decreases, following the same trend for SNR $\in [10, 30]$ dB. Note that the variances of $\hat{n}$ for the OCDM scheme are higher than those for the DMT scheme, even for higher levels of SNR.

Finally, this section compares the reference signals based on DMT and OCDM in terms of PAPR varying respectively the

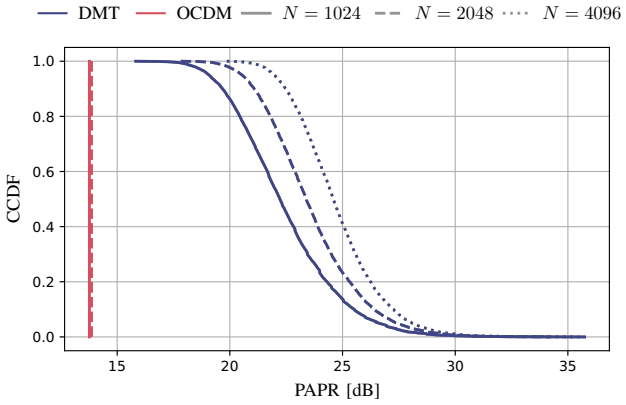

Fig. 6. CCDF of the PAPRs obtained from the symbol blocks for both DMT- and OCDM-based reference signals.

number of subcarriers and subchirps. This analysis considers the complementary cumulative distribution functions (CCDFs) of PAPR values obtained for $K = 10^4$ symbol blocks. The PAPR is expressed as

$$\text{PAPR} = \frac{\max|x_1[n]|^2}{E[|x_1[n]|^2]}, \tag{15}$$

where $E[\cdot]$ is the expected value and $\{x_1[n]\}_{n=0}^{N-1}$ is the first symbol block of each reference signal.

Fig. 6 shows the CCDF of PAPR values obtained for both DMT- and OCDM-based reference signals considering $N \in \{1024, 2048, 4096\}$. Note that, as the OCDM-based reference signal is fixed, see Eqs. (11) and (10), the CCDFs curves are vertical lines for all values of N and remain quite close to each other. On the other hand, for the DMT-based reference signal, which considered randomly generated BPSK symbols, the CCDFs show that the PAPR values rise as N increases. Also, the DMT-based reference signal presents much higher values of PAPR than the OCDM-based one. It is noteworthy that even using a brute-force algorithm, the minimum PAPR values for the DMT-based reference signal are around $3,\ 6$, and 12 dB higher than the ones found for the OCDM-based reference signal when $N = 1024,\ 2048$, and 4096, respectively.

VI. Conclusions

This paper has introduced an OCDM-based reference signal designed to accommodate the Schmidl & Cox symbol block synchronization technique within a PLC channel measurement methodology. Also, it has provided a performance comparison involving OCDM-based and DMT-based reference signals to assess the accuracy of the Schmidl & Cox synchronization technique when these reference signals are considered. Numerical results derived from a set of PLC channel measurements indicate that the OCDM-based reference signal is comparable to its DMT-based counterpart in terms of symbol block synchronization. Moreover, the OCDM-based reference signal exhibits lower PAPR values compared to the DMT-based reference signal. These results suggest that the OCDM-based reference signal could be integrated into the PLC channel measurement methodology, offering the advantage of lower PAPR for greater transmission efficiency and nonlinear distortion avoidance.

References

[1] H. C. Ferreira, L. Lampe, J. Newbury, and T. G. Swart, *Power Line Communications Theory and Applications for Narrowband and Broadband Communications over Power Lines*. Wiley & Sons, Incorporated, John, 2011.

[2] T. R. Oliveira, C. A. G. Marques, W. A. Finamore, S. L. Netto, and M. V. Ribeiro, "A methodology for estimating frequency responses of electric power grids," *Journal of Control, Automation and Electrical Systems*, vol. 25, no. 6, pp. 720–731, Sep. 2014.

[3] F. A. F. Villaça, Â. Camponogara, T. R. Oliveira, and M. V. Ribeiro, "Proposta de adaptação de uma técnica de sincronização de símbolo para aplicação em uma metodologia de medição de canais PLC," in *Brazilian Symposium on Telecommunications and Signal Processing*, Fortaleza, CE, Sep. 2021.

[4] T. M. Schimdl and D. C. Cox, "Robust frequency and timing synchronization for OFDM," *IEEE Transactions on Communications*, vol. 45, no. 12, pp. 1613–1621, Dec. 1997.

[5] X. Ouyang and J. Zhao, "Orthogonal chirp division multiplexing," *IEEE Transactions on Communications*, vol. 64, no. 9, pp. 3946 – 3957, Sep. 2016.

[6] L. de M. B. A. Dib, G. R. Colen, M. de L. Filomeno, and M. V. Ribeiro, "Orthogonal chirp division multiplexing for baseband data communication systems," *IEEE Systems Journal*, vol. 14, no. 2, pp. 2164–2174, Jun. 2020.

[7] M. de L. Filomeno, L. G. de Oliveira, Â. Camponogara, A. Diewald, T. Zwick, M. L. R. de Campos, and M. V. Ribeiro, "Joint channel estimation and Schmidl & Cox synchronization for OCDM-based systems," *IEEE Communication Letters*, vol. 26, pp. 1878 – 1882, Apr. 2022.

[8] J. M. Cioffi, "Advanced digital communications - chapter 4 (multichannel modulation)," arquivo PDF - disponível em https://cioffi-group.stanford.edu/ee379c/course_reader.html, 2007.

[9] M. S. Omar and X. Ma, "Designing OCDM-based multi-user transmissions," in *IEEE Global Communications Conference*, Dec. 2019, pp. 1–6.

[10] M. S. P. Facina, H. A. Latchman, H. V. Poor, and M. V. Ribeiro, "Cooperative in-home power line communication: Analyses based on a measurement campaign," *IEEE Transactions on Communications*, vol. 64, no. 2, pp. 778–789, Feb. 2016.